RSC Advances

PAPER

View Article Online
View Journal | View Issue

Cite this: *RSC Adv.*, 2025, **15**, 26302

Fluorescent imaging of glutathione distribution in frozen tissue slices based on TLC tracing technology†

Tatsuya Nishihara, ‡* Koki Nishida,‡ Rika Tsukame, Yumika Sugawara, Shunya Nagano and Kazuhito Tanabe *

The distribution of glutathione (GSH) in liver tissue is an important indicator for disease assessment. GSH depletion increases the susceptibility to oxidative stress and is involved in many diseases. Although mass spectrometry imaging (MSI) is a powerful tool for analysing the distribution of metabolites, it is difficult to image the distribution of reactive metabolites, such as the GSH bearing thiol group. In addition, MSI needs high-end instruments and takes a long time. In this study, we aimed to construct a methodology to trace GSH in frozen tissue slices onto a thin layer chromatography (TLC) plate by labelling with a fluorescent dye *in situ*. When a frozen tissue slice was attached to the functional TLC plate, the thiol-specific fluorescence labelling agent for TLC imaging (**tFLAT**) immediately reacted with GSH in the frozen liver tissue slice to produce a high-polarity GSH adduct (**tFLAT-GSH**). After the separation of unreacted **tFLAT** on the TLC plate by expansion using a low-polarity solvent, fluorescence signals derived from **tFLAT-GSH** were observed *in situ*. We also monitored the decrease in GSH in liver tissue slices when mice were treated with acetaminophen (APAP), which causes acute liver inflammation. The present method successfully detected GSH in the mouse liver tissue slices. This study provides a rational strategy for tracing target metabolites within frozen tissue slices on TLC plates for the first time.

Received 13th May 2025
Accepted 15th July 2025

DOI: 10.1039/d5ra03353e

rsc.li/rsc-advances

Introduction

Thiols play key roles in biological systems.[1] A variety of small molecular metabolites containing a thiol group exist in humans and animals, including cysteine (Cys), *N*-acetylcysteine, γ-glutamyl cysteine, cysteinyl glycine, homocysteine (Hcy), and glutathione (GSH). GSH is the most abundant intracellular thiol metabolite and plays an important role as an antioxidant.[2]

In the liver, hepatocytes supply GSH into the bloodstream to regulate the redox potential of the entire body.[3] The depletion of hepatic GSH is related to several liver diseases, such as drug-induced liver injury,[4] alcoholic/nonalcoholic fatty liver disease,[5] steatohepatitis,[6] liver fibrosis, and cirrhosis[7] due to increased susceptibility to oxidative stress. GSH is also known to contribute to drug metabolism in the liver through GSH conjugation.[8] Therefore, the distribution of GSH in the liver is a useful indicator for estimating the status of the liver tissue and the entire body.

Conventional analytical procedures have used tissue extracts to monitor metabolites, including GSH. While these methods have been useful, the problem is that they have irreversibly damaged the structural integrity of tissue samples.[9] Over the past few decades, mass spectrometry imaging (MSI) has been used to overcome this limitation. MSI is a powerful tool for metabolite analysis in frozen tissue slices and provides specific content information on several metabolites in certain locations with high spatial resolution (Fig. 1a).[10] MS equipped with matrix-assisted laser desorption/ionization (MALDI MSI) facilitates the analysis of a variety of molecules with high selectivity and offers a feasible sample preparation procedure.[11] Although several conventional matrices have been applied to image the GSH distribution in the tissue slice using MALDI-MSI,[12] direct analysis of thiol metabolites, including GSH, remains challenging due to their high reactivity. In recent years, some agents have been developed as MALDI probes to facilitate desorption/ionization by chemical labelling of tissues and these have been gradually applied in MSI studies for analytes of interest.[13] However, in principle, MSI requires high-end instruments and several hours are needed to analyse one slice. Therefore, a new methodology that enables the rapid and simple analysis of the spatial distribution of GSH in tissue slices is required.

To overcome this issue, we used a TLC plate. TLC is a widely-utilized analytical tool that enables rapid and simple separation of molecules on silica surfaces using only suitable solvents.

Department of Chemistry and Biological Science, College of Science and Engineering, Aoyama Gakuin University, 5-10-1 Fuchinobe, Chuo-ku, Sagamihara, Kanagawa, 252-5258, Japan. E-mail: nishihara@chem.aoyama.ac.jp; tanabe.kazuhito@chem.aoyama.ac.jp

† Electronic supplementary information (ESI) available. See DOI: https://doi.org/10.1039/d5ra03353e

‡ These authors contributed equally to this work.

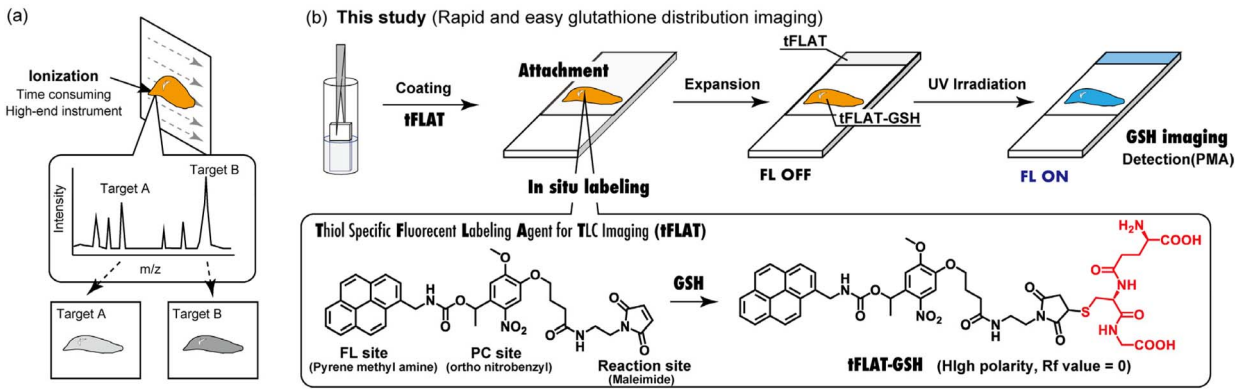

Fig. 1 Schematic illustration of (a) mass spectrometry imaging and (b) glutathione (GSH) imaging using the thiol specific fluorescence labelling agent for TLC imaging (**tFLAT**).

Additionally, the separation characteristics can be precisely controlled through silica surface modifications and the choice of solvent. Considering these characteristics, in this study, we propose a method for imaging the distribution of GSH in tissue slices using a functional TLC plate (Fig. 1b). We designed a thiol-specific fluorescent labelling agent for TLC imaging (**tFLAT**) consisting of a fluorescent dye site (FL site, pyrene methylamine, **PMA**), a photocleavable site (PC site, *ortho*-nitrobenzyl), and a reaction site (maleimide). Analysis of the GSH distribution in liver tissue slices was performed in three steps. First, frozen liver tissue slices were attached to a functional TLC plate coated with **tFLAT**. The Michael addition reaction between **tFLAT** and GSH in the tissue proceeded on a TLC plate to yield the highly polar product, **tFLAT-GSH**. Next, the unreacted **tFLAT** was removed from the tissue-attached area on TLC plate by expansion in a low-polarity solvent. Finally, the fluorescent dye, **PMA**, was released by photoirradiation. Based on the fluorescent signal after the photoirradiation derived from the **tFLAT-GSH**, the location and amount of GSH in the tissue could be visualised. GSH imaging in liver tissue was successfully achieved using a functional TLC plate for the first time. We also demonstrated that it was possible to monitor the depletion of GSH in the liver tissue due to acute hepatitis induced by acetaminophen (APAP).

Experimental

Synthesis of tFLAT

A solution of photocleavable linker (32.2 mg, 57.2 μmol) and **PMA** (15.1 mg, 65.3 μmol) was stirred for 30 min in dry DMF (1.5 mL) under N_2 atmosphere at ambient temperature (Scheme S1†). The reaction mixture was extracted with EtOAc. Then, the organic layer was washed with brine and dried over $MgSO_4$ and evaporated to dryness. The crude product was purified by silica gel column chromatography ($CHCl_3$/MeOH = 20/1) to give **tFLAT** (26.4 mg, 68%) as pale yellow solid.: MP. 158.5–160.5 °C; ^{1}H NMR (DMSO-d_6, 500 MHz) δ 8.30–7.93 (m, 11H), 7.58 (s, 1H), 7.13 (s, 1H), 6.96 (s, 2H), 6.17 (q, 1H, J = 6.0 Hz), 4.88 (m, 2H), 4.02 (t, 2H, J = 6.5 Hz), 3.75 (s, 3H), 3.44 (t, 2H, J = 5.8 Hz), 3,19 (m, 2H), 2.15 (t, 2H, J = 7.3 Hz), 1.90 (m, 2H), 1.55 (d, 3H, J = 6.0 Hz); ^{13}C NMR (DMSO-d_6, 125 MHz) δ 171.7, 171.0, 155.4, 153.6, 146.8, 139.3, 134.5, 133.4, 132.8, 130.7, 130.2, 130.1, 127.9, 127.5, 127.3, 127.0, 126.3, 126.2, 125.3, 125.2, 124.6, 124.0, 123.9, 123.0, 108.5, 108.3, 68.2, 67.5, 56.0, 42.0, 37.2, 36.9, 31.6, 24.5, 21.8; FABMS (NBA) m/z 679 [(M + H)$^+$]; HRMS calcd. for $C_{37}H_{34}N_4O_9$ [(M + H)$^+$] 679.2399, found 679.2405.

Agarose gels containing GSH stamp on fTLC and quantification of tFLAT-GSH

To prepare 2% agarose gels, 1.0 g agarose and 45 mL milliQ water were mixed and heated to dissolve agarose with a microwave oven. Next, 9 mL agarose solution was poured into a mold (4.2 cm × 3.8 cm). For evaluation of GSH dose dependency: 1 mL of 0, 0.5, 1 or 2 mM GSH in 100 mM phosphate buffer (pH 7.4) were poured into the molds and mixed well. Finally, the gels were washed with millQ and cut into 1/16 portion (10.5 mm × 9.5 mm × 5.5 mm). The gels were stamped onto the functional TLC plates coated with **tFLAT** for 5 s. Then the TLC plate was dried in a desiccator linked with a vacuum compressor for 1 h. The dried TLC plate was expanded with moving phase $CHCl_3$/MeOH (4/1). Subsequently, the TLC plate was irradiated by UV light (365 nm) for 20 min. Finally, glass side of TLC plates were imaged using FluoroPhoreStar3000.

Preparation of APAP-induced liver injury model mice

Two groups of mice (10 weeks old, 27.6–30.2 g; APAP (−), n = 2; APAP (+), n = 3) were fasted for 5 h. One group was injected intraperitoneally with 30 mg mL^{-1} APAP dissolved in D-PBS at an overdose level (300 mg kg^{-1} body weight). The other group was injected an equivalent volume of D-PBS intraperitoneally as a control. After injection, mice were allowed free access to water and food. After 2 h of injection, the livers and blood were collected from the mice under anesthesia with isoflurane (MSD Animal Health).

Detection of GSH in mouse liver tissue sections

TLC plates (7.5 cm × 2.0 cm) were dipped into 0.5 mM **tFLAT** in chloroform solution for 2 times. The preparation and attachment of tissue sections onto the TLC plates were commissioned

to Pharma Foods, Inc. Tissue sections of injury and normal livers (10 μm) were attached to **tFLAT**-coated TLCs. The TLCs were heated on a hot plate from the glass side (100 °C, 15 s) to adhere the tissue sections. After drying, the TLC plate was developed using $CHCl_3$/MeOH (4/1) solution. Subsequently, the TLC plate was irradiated by UV light (365 nm) for 20 min. Fluorescence intensity imaging was performed using hyperspectral camera NH-8 and UV lamp (EBA JAPAN Co., Ltd).

Results and discussion

Synthesis and characterization of tFLAT

The **tFLAT** was synthesized (Scheme S1†) and its optical properties were evaluated (Fig. 2a). The **tFLAT** was dissolved in a dimethylsulfoxide (DMSO) solution, the samples were irradiated with 365 nm UV light for 0 or 7.5 min, and the absorbance and fluorescence spectra were measured (Fig. 2b). Before the photocleavage reaction, the fluorescence signal was quenched by the nitrobenzyl moiety,[14] while the photocleavage reaction of the *ortho*-nitrobenzyl group resulted in a fluorescence emission from the released **PMA**. The **PMA**-derived fluorescence signal was observed after photo-irradiation (Fig. 2b). The photocleavage reaction was then examined using TLC plate. **PMA**-derived fluorescence signals were observed in the spotted area of **tFLAT** after photoirradiation (Fig. 2c). The fluorescence emission of **PMA** on the TLC plate increased with the increasing amount of **tFLAT** (Fig. 2d, e and S1†). Thus, we could quantify the amount of **tFLAT**-adduct using **PMA** fluorescence after the photocleavage reaction.

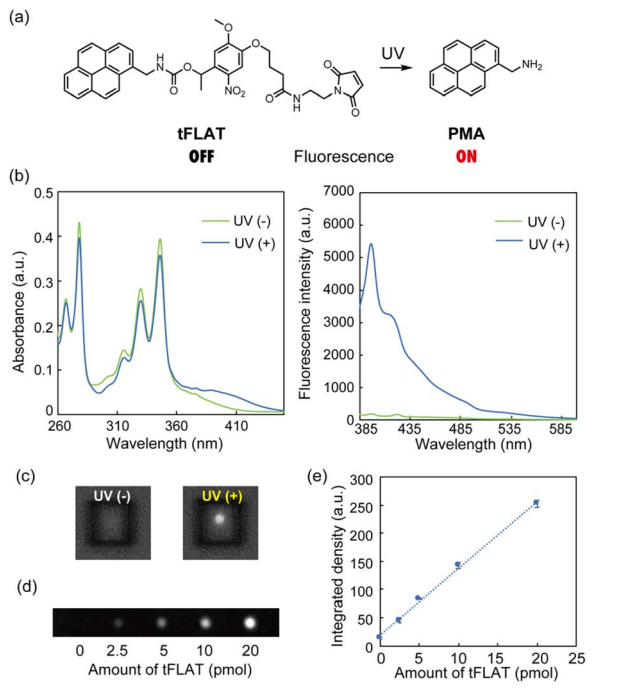

Fig. 2 Characterization of **tFLAT**. (a) Photo cleavage reaction to release the **PMA**. After the photo irradiation, the fluorescence from **PMA** was recovered. (b) Absorbance (left) and fluorescence spectra (right E_x = 375 nm) of 10 μM **tFLAT** in DMSO with or without photo irradiation (365 nm, 0 or 7.5 min). (c) Representative fluorescence image of **tFLAT** (500 pmol) on TLC plate. (d) Representative fluorescence image of **tFLAT** (0, 2.5, 5, 10 or 20 pmol) on a TLC plate. (e) Calibration curve using **tFLAT**. Data = mean ± SD (n = 3).

Michael addition reaction on the TLC plate using GSH

The reactivity between **tFLAT** and GSH on the TLC plate was evaluated by spotting the GSH solution (0–20 pmol) onto a functional TLC plate coated with **tFLAT** (Fig. 3a). After drying the spotted TLC plate, expansion was performed using a mixture of chloroform and methanol (4 : 1) to separate the unreacted **tFLAT** (Fig. S2†). Under these separation conditions, the **tFLAT-GSH** was retained in the spotted area, whereas unreacted **tFLAT** was removed. We also confirmed that the fluorescence intensity increased in a dose-dependent manner. The reaction rate was determined by monitoring fluorescence signals. Approximately 25% of the spotted GSH reacted with **tFLAT** on the TLC plate (Fig. 3b and c).

Evaluation of GSH tracing using agarose gel

Agarose gel was used as a tissue model to verify whether GSH imaging could be achieved using a functional TLC plate coated with **tFLAT** (Fig. 3a). Agarose gel containing GSH (0–125 nmol) was stamped for 5 s to allow the Michael addition reaction on the **tFLAT**-coated TLC plate. After expansion, we confirmed that **tFLAT-GSH** was retained in the *in situ* labelling position, whereas unreacted **tFLAT** was removed. We also observed fluorescent signals derived from released **PMA** after the TLC plate was irradiated with UV light. The results of the GSH imaging are shown in Fig. 3d. No fluorescence signal was observed when agarose gel without GSH was stamped, whereas a fluorescence signal corresponding to the shape of the agarose gel was observed when GSH was present in the gel. The fluorescence intensity increased linearly with an increase in the amount of GSH in the agarose gel (Fig. 3e). The **tFLAT-GSH** amount was determined using a calibration curve of **tFLAT**, and we confirmed that 0.4% of the GSH in the entire agarose gel (10.5 mm × 9.5 mm × 5.5 mm) reacted with **tFLAT** on the TLC plate. These results indicate that the GSH on the surface of the agarose gel could be traced to the functional TLC plate using the Michael reaction. We also conducted GSH imaging using agarose gels at different pH values. We confirmed that the reactivity on TLC plate was similar under both weakly-acidic and weakly-basic conditions, suggesting that the reaction was independent of pH conditions (Fig. S3†).

Fluorescent imaging of GSH distribution in frozen liver tissue using functional TLC plate coated with tFLAT

Having confirmed the feasibility of the quantitative detection of GSH using TLC tracing, the method was used in frozen liver tissue, which is rich in GSH and plays a crucial role in drug metabolism through GSH conjugation.[8] As described above, the GSH imaging in the liver was used to evaluate the status of GSH in liver tissue and entire body. To trace metabolites from the frozen tissue slice onto functional TLC plate, a 10 μm thick tissue section was directly attached to the TLC plate and allowed to react with **tFLAT** (Fig. 4a and b). Because **tFLAT** is designed to

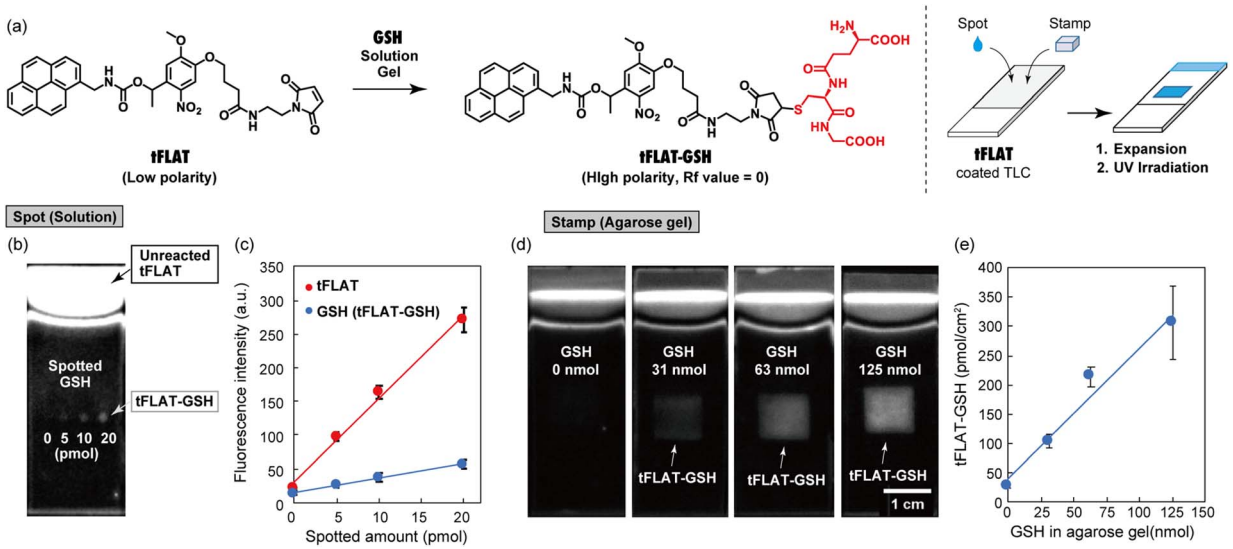

Fig. 3 Conversion rate from **tFLAT** to **tFLAT-GSH** on TLC plate. (a) Schematic illustration of Michael addition on the TLC plate by spotting the GSH solution and procedure for GSH imaging. (b) Representative **PMA** fluorescence image from TLC plate. Spotted **tFLAT** : **tFLAT** (0, 5, 10, or 20 pmol) was spotted on normal TLC plate. Spotted GSH : GSH (0, 5, 10, or 20 pmol) in phosphate buffer (10 mM, pH 7.4) were spotted on **tFLAT**-coated TLC plate. (c) The relationship between the amount of **tFLAT** or GSH and its fluorescence intensity from **tFLAT** and **tFLAT-GSH**. (d) Representative results of GSH imaging using functional TLC plate coated with **tFLAT**. The **tFLAT**-coated TLC plate was stamped by agarose gel containing GSH (0, 31, 63 or 125 nmol in 10 mM phosphate buffer pH 7.4) for 5 s. After the separation of unreacted **tFLAT** and photo irradiation (20 min), the fluorescence from TLC plate was observed using FluoroPhoreStar3000. (e) Relationship between amount of GSH in agarose gel and **tFLAT-GSH** amount per cm^2. The images were analyzed using Image J. Data are means ± SD ($n = 3$).

emit fluorescence only upon photoirradiation, the fluorescence before and after irradiation was measured after the expansion process and the **tFLAT-GSH**-derived fluorescence was determined based on the difference. When analysing tissue samples, autofluorescence from endogenous molecules poses a barrier to the detection of **tFLAT-GSH**-derived fluorescence. A hyperspectral camera was used to minimise the influence of autofluorescence and maximise the detection of **tFLAT-GSH**-derived fluorescence. The camera acquired the fluorescence spectra for each pixel, enabling signal intensity measurements at wavelengths where autofluorescence was weak and **tFLAT-GSH**-derived fluorescence was strong (Fig. S4†).

Analysis of the fluorescence spectra before and after UV irradiation indicated that the fluorescence intensity at 450 nm effectively detected **tFLAT-GSH**-derived fluorescence signals (Fig. S5†). When measuring the difference in the fluorescence intensity at 450 nm before and after UV irradiation, strong fluorescence signals were obtained from the tissue-attached area. After expansion and subtracting the background signal, **tFLAT-GSH**-derived fluorescence was accurately determined (Fig. 4c and S6†). In addition, it is documented that GSH exists at 1–10 mM in physiological conditions, whereas cysteine and homocysteine are present at much lower concentrations of 240–360 and 12–15 μM, respectively.[15] Therefore, the observed fluorescence signal is considered to predominantly reflect the presence of GSH. When the control experiment was performed using TLC plate without **tFLAT**-coating, no difference in the fluorescence intensity was observed, even within the tissue-attached area (Fig. S7†). Therefore, the difference in fluorescence intensity at 450 nm could be attributed to the reaction between thiols in the liver tissue and **tFLAT** on the TLC plate.

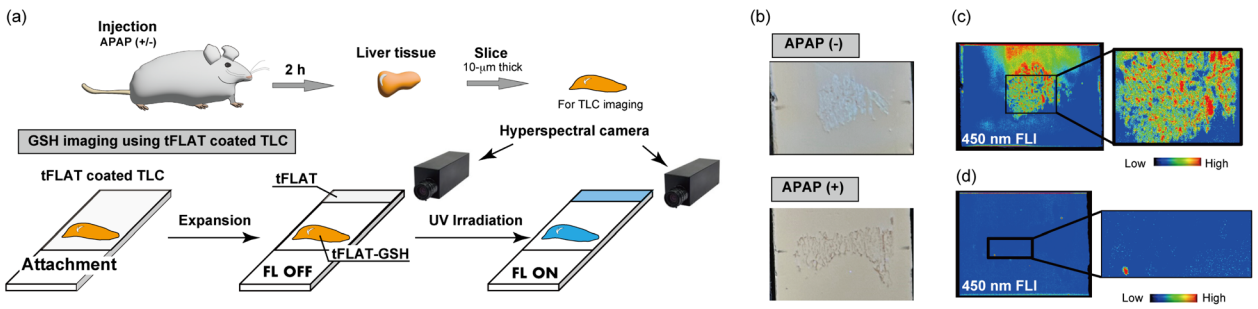

Fig. 4 (a) Schematic illustration of GSH imaging in the frozen liver tissue using **tFLAT** coated TLC plate and hyperspectral camera. (b) Photograph of tissue attached functional TLC plate. (c) Fluorescent intensity imaging at 450 nm of (c) normal liver tissue slice and (d) acute hepatitis slice.

Next, we monitored changes in GSH levels in the liver tissue that varied with drug administration. APAP was selected as the drug to decrease the GSH level in the liver tissue. It is well-documented that excess APAP cannot be metabolised by glucuronidation or sulphate conjugation and is converted by cytochrome P450 to the highly reactive *N*-acetyl-benzoquinoneimine (NAPQI), which is then converted to the GSH-conjugated form for detoxification. Thus, GSH in the liver tissue is depleted, resulting in liver damage due to cytotoxicity derived from NAPQI.[16] Based on a previous study that showed GSH fluctuation in the liver using APAP treatment, we injected an excessive dose of APAP intraperitoneally.[16] Then, 2 h after administration, ALT in plasma and GSH in liver tissue were measured to confirm the occurrence of liver injury and depletion of GSH (Fig. S8 and S9†). When monitoring **tFLAT-GSH**-derived fluorescence signals in the liver, almost no fluorescence was detected in the tissue-attached area on TLC plate, unlike the control conditions without APAP treatment (Fig. 4d). It should be noted, however, that the efficiency of the reaction may vary depending on the region of the tissue. Nevertheless, considering the quantified GSH values in the tissue lysate, it is likely that the fluctuations in tissue GSH levels were successfully analysed by this method. Thus, we could image GSH levels changed by APAP administration in the liver tissue.

In a separate experiment, we applied the present system to the analysis of multiple thiol metabolites. We investigated the labelling reaction of **tFLAT** by other thiol metabolites, because **tFLAT** has a maleimide group as the reaction point that can react with every thiol group. We embedded the mouse-derived tissues in the OCT compound and created 2 mm thick frozen liver tissue sections using a custom-made tissue slicer for stamping (Fig. S10†). Frozen liver tissue slices were stamped onto a **tFLAT**-spotted TLC plate, and the adducts were expanded using a mixture of BuOH, AcOH, and H_2O (4 : 1 : 1). After separation, UV light was applied to release **PMA** and detect the labelled thiol metabolites. We also conducted a similar analysis using frozen kidney tissue to compare the thiol metabolites in liver and kidney. In the liver tissue, we found only one new spot that was assigned to **tFLAT-GSH** (Fig. S11†). A new spot derived from the cysteine adduct (**tFLAT-Cys**) was observed when the same experiment was performed on frozen kidney tissue slices. These results strongly indicate that the present system using TLC can distinguish thiol metabolites in the tissue. Accordingly, the supplementary dot-spot assay provides key information regarding thiol composition in tissues; if multiple thiol species are detected, it is essential to consider how this compositional diversity may impact the assay outcomes.

Conclusions

In this study, we developed a rapid and simple methodology to analyze the location and amount of the target metabolite, GSH, in frozen liver tissue and demonstrated GSH imaging in liver tissue using functional TLC plate for the first time. To determine the presence of GSH in the tissue, frozen liver tissue slices were attached onto **tFLAT**-coated TLC plates, and the fluorescent signals derived from **tFLAT-GSH** after UV irradiation were tracked. The fluorescence signal derived from **tFLAT-GSH** was successfully detected on a TLC plate because of the efficient coupling reaction between **tFLAT** and GSH in the tissue slice. We also visualized GSH fluctuations in the tissue due to an overdose of APAP. In this study, our strategy was demonstrated specifically for the detection of glutathione in frozen liver tissue slices. Further studies will be required to evaluate the applicability of this approach to other tissue types and to the detection of additional disease-related biomarkers using appropriate labelling strategies. From the perspective of molecular design, a fluorescent labelling agent can be designed using the polarity change upon reaction with the target molecule. Therefore, it is expected to be widely applicable to various molecular species.

Ethical statement

All experiments involving animals were performed according to the Institutional Guidance of the Aoyama Gakuin University on Animal Experimentation with permission from the Animal Experiment Committee of the Aoyama Gakuin University.

Data availability

All the data have been presented in the manuscript and ESI.†

Author contributions

T. N. conceived and designed the study. T. N., K. N., and R. T. designed the experiments. K. N. and S. N. synthesized the compounds. T. N., K. N., R. T., and Y. S. conducted biological experiments and analyses. T. N., K. N., and K. T. wrote the manuscript, which was edited by all coauthors.

Conflicts of interest

There are no conflicts to declare.

Acknowledgements

The hyperspectral camera imaging and analysis were performed by Mr Sawaka Kako and Mr Hironori Sakamoto of EBA JAPAN Co., Ltd. We appreciate their assistance in this study. This research was supported by JSPS KAKENHI [grant numbers 23K04966 (to T. N.) and 23K26779 (to K. T.)], the Astellas Foundation for Research on Metabolic Disorders (to T. N.), and the Aoyama Gakuin University Research Institute (to K. T. and T. N.).

References

1 X. Chen, Y. Zhou, X. Peng and J. Yoon, *Chem. Soc. Rev.*, 2010, **39**, 2120–2135, DOI: **10.1039/b925092a**.
2 C. Hwang, A. J. Sinskey and H. F. Lodish, *Science*, 1992, **257**, 1496–1502, DOI: **10.1126/science.1523409**.
3 (*a*) N. Kaplowitz, T. Y. Aw and M. Ookhtens, *Annu. Rev. Pharmacol. Toxicol.*, 1985, **25**, 715–744, DOI: **10.1146/**

annurev.pa.25.040185.003435; (*b*) N. Kaplowitz, *Yale J. Biol. Med.*, 1981, **54**, 497–502.

4 (*a*) J. R. Mitchell, D. J. Jollow, W. Z. Potter, J. R. Gillette and B. B. Brodie, *J. Pharmacol. Exp. Ther.*, 1973, **187**, 211–217; (*b*) A. U. Lee and G. C. Farrell, *J. Hepatol.*, 2001, **35**, 756–764, DOI: 10.1016/S0168-8278(01)00196-9.

5 (*a*) T. Hirano, N. Kaplowitz, H. Tsukamoto, S. Kamimura and J. C. Fernandez-Checa, *Hepatology*, 1992, **16**, 1423–1427, DOI: 10.1002/hep.1840160619; (*b*) J. C. Fernandez-Checa and N. Kaplowitz, *Toxicol. Appl. Pharmacol.*, 2005, **204**, 263–273, DOI: 10.1016/j.taap.2004.10.001.

6 (*a*) A. P. Rolo, J. S. Teodoro and C. M. Palmeira, *Free Radical Biol. Med.*, 2012, **52**, 59–69, DOI: 10.1016/j.freeradbiomed.2011.10.003; (*b*) J. Garcia-Ruiz and J. C. Fernandez-Checa, *J. Gastroenterol. Hepatol.*, 2006, **21**, S3–S6, DOI: 10.1111/j.1440-1746.2006.04570.x.

7 E. Purucker, R. Winograd, E. Roeb and S. Matern, *Exp. Med.*, 1998, **198**, 167–174, DOI: 10.1007/s004330050100.

8 M. Vairetti, L. G. Di Pasqua, M. Cagna, P. Richelmi, A. Ferrigno and C. Berardo, *Antioxidants*, 2021, **10**, 364, DOI: 10.3390/antiox10030364.

9 (*a*) L. Chang, F. Lin, K. Cheng, J. Li, X. Sun, D. Figeys, J. Jiang, Y. Ye and J. Liu, *Anal. Chim. Acta*, 2021, **1184**, 339016, DOI: 10.1016/j.aca.2021.339016; (*b*) S. Kumari, A. Ali, T. Roome, A. Razzak, A. Iqbal, A. J. Siddiqui, S. M. Z. Azam, H. Shaikh, H. R. El-Seedi and S. G. Musharraf, *Arabian J. Chem.*, 2021, **14**, 102907, DOI: 10.1016/j.arabjc.2020.11.013.

10 (*a*) R. M. Caprioli, T. B. Farmer and J. Gile, *Anal. Chem.*, 1997, **69**, 4751–4760, DOI: 10.1021/ac970888i; (*b*) S. L. Luxembourg, T. H. Mize, L. A. McDonnell and R. M. A. Heeren, *Anal. Chem.*, 2004, **76**, 5339–5344, DOI: 10.1021/ac049692q.

11 (*a*) L. Ling, C. Xiao, Y. Ma, L. Jiang, S. Wang, L. Guo, S. Jiang and X. Guo, *Anal. Chem.*, 2019, **91**, 8801–8807; (*b*) L. Ling, L. Jiang, Q. Chen, B. Zhao, Y. Li and X. Guo, *Food Chem.*, 2021, **340**, 128208, DOI: 10.1016/j.foodchem.2020.128208; (*c*) Y. Liu, L. Chen, L. Qin, M. Han, J. Li, F. Luo, K. Xue, J. Feng, Y. Zhou and X. Wang, *Chem. Commun.*, 2019, **55**, 12559–12562, DOI: 10.1039/c9cc06961e; (*d*) B. Li, R. Sun, A. Gordon, J. Ge, Y. Zhang, P. Li and H. Yang, *Anal. Chem.*, 2019, **91**, 8221–8228, DOI: 10.1021/acs.analchem.9b00803; (*e*) H. Liu, M. Han, J. Li, L. Qin, L. Chen, Q. Hao, D. Jiang, D. Chen, Y. Ji, H. Han, C. Long, Y. Zhou, J. Feng and X. Wang, *Anal. Chem.*, 2021, **93**, 11920–11928, DOI: 10.1021/acs.analchem.0c05480; (*f*) H. Liu, R. Chen, J. Wang, S. Chen, C. Xiong, J. Wang, J. Hou, Q. He, N. Zhang, Z. Nie and L. Mao, *Anal. Chem.*, 2014, **86**, 10114–10121, DOI: 10.1021/ac5034566; (*g*) J. Wang, C. Wang and X. Han, *Anal. Chim. Acta*, 2018, **1000**, 155–162, DOI: 10.1016/j.aca.2017.09.046.

12 M. G. Nye-Wood, J. M. Spraggins, R. M. Caprioli, K. L. Schey, P. J. Donaldson and A. C. Grey, *Exp. Eye Res.*, 2021, **154**, 70–78, DOI: 10.1016/j.exer.2016.11.008.

13 (*a*) M. Shariatgorji, A. Nilsson, E. Fridjonsdottir, T. Vallianatou, P. Källback, L. Katan, J. Sävmarker, I. Mantas, X. Zhang, E. Bezard, P. Svenningsson, L. R. Odell and P. E. Andrén, *Nat. Methods*, 2019, **16**, 1021–1028, DOI: 10.1038/s41592-019-0551-3; (*b*) T. Iwama, K. Kano, D. Saigusa, K. Ekroos, G. van Echten-Deckert, J. Vogt and J. Aoki, *Anal. Chem.*, 2021, **93**, 3867–3875, DOI: 10.1021/acs.analchem.0c04479; (*c*) S.-S. Wang, Y.-J. Wang, J. Zhang, T.-Q. Sun and Y.-L. Guo, *Anal. Chem.*, 2019, **91**, 4070–4076, DOI: 10.1021/acs.analchem.8b05680.

14 R. T. Cummings and G. A. Krafft, *Tetrahedron Lett.*, 1988, **29**, 65–68.

15 N. Kaushik, V. Nehra, P. Novakova and P. Zimcik, *ACS Omega*, 2022, **8**, 98–126.

16 (*a*) M. R. McGill, M. Lebofsky, H. R. Norris, M. H. Slawson, M. L. Bajt, Y. Xie, C. D. Williams, D. G. Wilkins, D. E. Rollins and H. Jaeschke, *Toxicol. Appl. Pharmacol.*, 2013, **269**, 240–249, DOI: 10.1016/j.taap.2013.03.026; (*b*) R. D. Beger, S. Bhattacharyya, X. Yang, P. S. Gill, L. K. Schnackenberg, J. Sun and L. P. James, *Arch. Toxicol.*, 2015, **89**, 1497–1522, DOI: 10.1007/s00204-015-1519-4.